A Methodology to Investigate Skin-Stringer Separation in Postbuckled Composite Stiffened Panels

Kootte, Luc; Bisagni, Chiara

DOI
10.2514/6.2020-0477

Publication date
2020

Document Version
Final published version

Published in
AIAA Scitech 2020 Forum

AIAA SciTech Forum
6-10 January 2020, Orlando, FL
AIAA Scitech 2020 Forum

10.2514/6.2020-0477

A Methodology to Investigate Skin-Stringer Separation in Postbuckled Composite Stiffened Panels

Lucas J. Kootte[1] and Chiara Bisagni[2]
Delft University of Technology, Delft, 2629HS, Netherlands

A methodology is presented to investigate and improve the strength and damage tolerance of stiffened composite panels used in aerospace structures subjected to postbuckling deformation. These structural panels have the capability to operate in the postbuckling field, but the possible interaction between the postbuckling deformation and the damage initiation and propagation is yet to be fully understood. The developed methodology considers single-stringer specimens representative of stiffened panels to analyze skin-stringer separation. In this paper single-stringer specimens are studied in a four-point twisting configuration in order to investigate the region of maximum twisting, where the separation between the skin and the stiffener can initiate. A new test set-up is presented that recreates the four-point layout that can trigger separation due to twisting. The applied methodology shows that it is possible to mimic the out-of-plane buckling deformation of a large panel and study this numerically and experimentally through a single-stringer specimen.

I. Introduction

To design aeronautical composite stiffened panels that can safely operate in a postbuckled state, the interaction of the large postbuckling deformation of the skin with the complex failure modes inherent to composites needs to be fully understood. Unstable skin-stringer separation is one of the most critical failure modes, since the postbuckling deformation of the skin can result in the opening of the skin-stringer interface, especially in the presence of impact damage or manufacturing defects.

In recent literature, a number of studies regarding different methods to investigate skin-stringer separation in a simplified manner have been reported [1-5]. Among the reported tests, the three- and four-point bending tests are the most common test configurations. However, a major drawback of these tests is the dependency of the fracture toughness on the width of the specimen. The cracking within the interface nucleates at the free edge and is therefore not representative of the failure that occurs in a multi-stringer panel. To solve this problem, a seven-point bending test rig was designed by NLR [6] to reproduce the symmetric buckling shape that results from the compression of a stiffened panel. The seven-point bending test consists of a single-stringer specimen, where five supports and two loading points apply out-of-plane deformation to the skin. This type of loading mimics the buckling deformation, allowing the study of the complex interaction between the buckling deformation and the interlaminar damage propagation. Bertolini et al. [7-8] showed that this can be used both for symmetrical and skewed buckling. Recently, NASA performed seven-point bending tests as part of the Advanced Composite Consortium (ACC) program [9-12].

In the analyses of multi-stringer panels, the first and most common delamination mode initiates on the edge of the stiffener flange and is induced by buckling that occurs in the skin, which tends to pull away the skin from the stringer flange. This failure mechanism is mainly governed by delamination mode I. Every so often, a different failure mechanism can initiate where the delamination may develop with respect to the nodal line or inflection point in buckling, driving the failure mechanism as a combination of modes II + III [8, 13-16]. The mode III critical strain energy release rate has been studied using an Edge Crack Torsion (ECT) coupon test [17-20] for composite interfaces.

The work presented in this paper concerns the development of a methodology that enables the in-depth study of critical bucking mode and its interaction with skin-stringer separation in a multi-stringer panel. More details on this interaction can be obtained by studying this phenomenon on a single-stringer panel, both numerically and

[1] PhD Student, Faculty of Aerospace Engineering, AIAA Student Member.
[2] Professor, Faculty of Aerospace Engineering, AIAA Associate Fellow.

experimentally. The paper focuses on a single-stringer specimen under a novel four-point loading configuration, which is inspired by the ECT test.

II. Methodology

A building block approach has been introduced to meet the needs of a standardized testing approach that would reduce the costs and risk of the design of a composite structure [21]. Testing is required to validate the structural behavior for certification. Testing is conducted on multiple levels, with increasing size/complexity, within this context simplified to: coupons, single-stringer specimens and multi-stringer panels. An increase in size and complexity is accompanied by an increase in costs. On all these levels, numerical analyses are also conducted, which can provide more detail about the structure. Furthermore, it can prevent the use of multiple experimental set-ups and the number of configured structural panels required for testing. Additionally, it should increase the number of considered parameters and loading cases that can be investigated while reducing costs. An optimum has to be found between the costs related to testing in a certain level and the reliability of the outcome.

The single-stringer specimens, in between the complexity and size of the coupon specimens and multi-stringer panels, currently lacks a standardized testing approach. This is particularly true when buckling is considered, where separation between the stringer and skin can be a critical failure mechanism. The presented methodology, which is under development, bridges the gap between the coupon and multi-stringer panel level in the building block approach. It consists of a modelling and experimental approach that can be used in the design of composite stiffened panels to determine the strength and damage tolerance related to skin-stringer separation. An overview of the methodology is presented using the building block pyramid in Fig. 1.

The material parameters obtained from coupon tests are used to develop a model of a multi-stringer panel. These parameters are the Young's modulus, shear modulus and Poisson's ratio for the intralaminar properties and the critical Strain Energy Release Rate (SERR) and interface strength for the interlaminar properties. The buckling response of a multi-stringer panel loaded under compression is considered in this investigation. The critical buckling shapes and the expected locations where the skin-stringer separation may occur were obtained. These can be the location of maximum twisting or maximum bending. In order to gain a better understanding of the interaction between the skin-stringer separation and buckling deformation efficiently, a single-stringer representation of the multi-stringer panel is designed [22] as shown in Fig. 1.

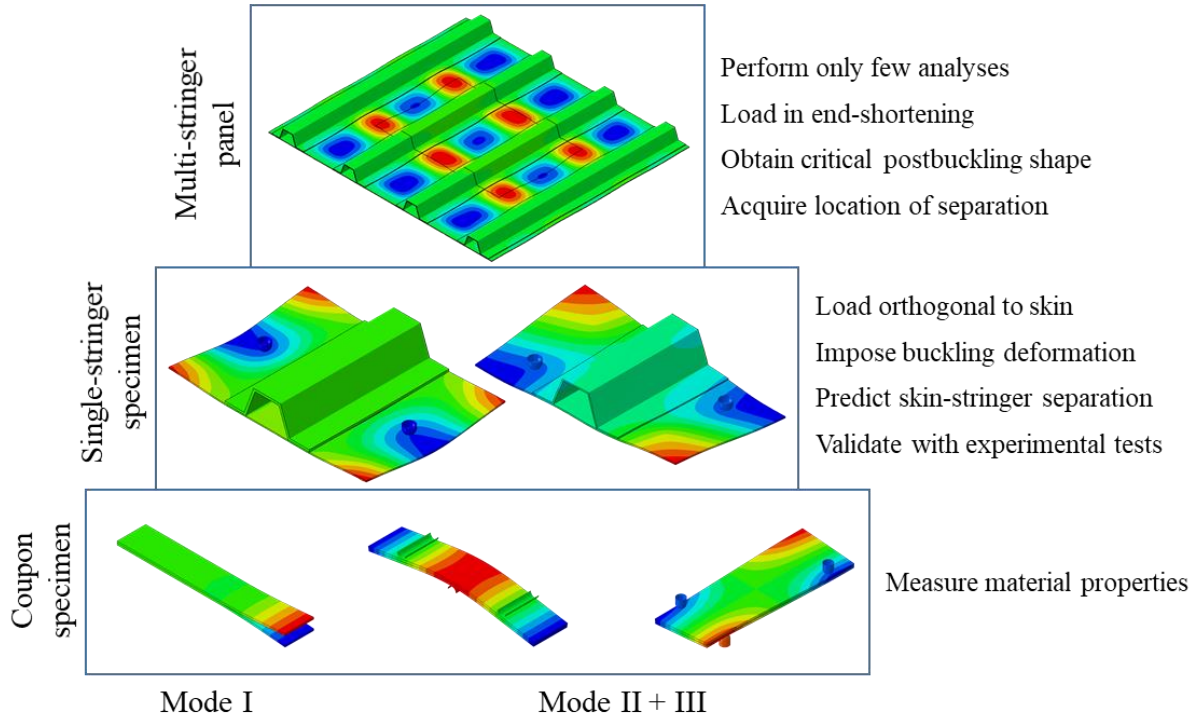

Fig. 1 Building block pyramid for the developed methodology.

By loading a single-stringer specimen perpendicular to the skin plane, the out-of-plane buckling deformation of a multi-stringer panel can be duplicated. The goal is to achieve the best approximation of the buckling deformation by studying the configuration of the supports and loading points that apply the load on the single-stringer specimen. By comparing each configuration to the region of interest in the multi-stringer panel, an optimum can be found. In current simulations, the Finite Element (FE) model of the single-stringer specimens does not require any damage models since the focus is only on generating the out-of-plane deformation.

The concept described above is applied to a single-stringer panel loaded in twisting to duplicate the inflection point regions. However, it can also be applied to the skin-stringer separation dominated by mode-I type delaminations. In this case, the seven-point bending layout would be used as a basis. Even so, the same procedure can be applied by changing the position of the supports and loading points in order to obtain the optimal seven-point bending configuration. An example of both the seven-point and four-point layout and their resulting imposed buckling deformation can be seen on the single-stringer specimen level in the building block approach in Fig. 1.

The plan is to use the experimental results and validate the numerical models using an adaptive multi-point test equipment. This equipment is designed such that the number and position of the supports and loading points can be changed in order to create different bending configurations such as four-point or seven-point bend setup. The position of the supports and loading points obtained from the FE study can be duplicated exactly. Digital Image Correlation (DIC) and non-destructive inspections with ultrasonic C-scan are used to collect the deformation patterns and damage information, respectively. The objective is to obtain the detailed characterization of the separation mechanisms at the skin-stringer interface.

III. Skin-Stringer Separation in a Four-Stringer Composite Panel

This section discusses the multi-stringer sub-structural panel that is loaded in postbuckling. The layup of the panel, material data, geometry and the finite element implementation are described in this section.

The composite structure of interest is a four-stringer panel, which is illustrated in Fig. 2, and it is made of IM7/977-3 [23] carbon/epoxy, where the skin and stringer are co-cured. The material properties can be found in Table 1, where the mode II interlaminar properties are also used for mode III. The panel dimensions are 685 mm, and 770 mm in length and width, respectively. The width of the skin bay between two stringers is 100 mm for the outer two bays and 105 mm for the central bay. The slightly larger bay width assures that buckling and consequently skin-stringer separation initiates at the central bay. In order to reduce the formation of thermal strains upon curing of the single-stringer specimens, a symmetric layup for both the skin and stringer was selected $[-45/45/0/90/-45/45]_s$ and $[45/-45/0/90/45/-45]_s$, respectively. The anti-symmetric layup for the skin-stringer overlap assures a mismatch in stiffness at the skin-stringer interface.

The numerical model of the four-stringer panel is developed in Abaqus 2019 [24] with the use of eight-node continuum shell element (SC8R). In order to reduce the required computational resources, the four-stringer panel is divided into two sections, namely the inner and outer section. Skin-stringer separation is expected to occur primarily in the inner section due to the larger central skin bay. Consequently, the outer section does not require a damage model, but simply a rigid tie constraint between the skin and stringer, which prohibits any form of separation. The element size in the outer section is 5 mm, based on a buckling eigenvalue convergence study. The two sections are coupled using a surface to surface rigid tie constraint, which is highlighted by the close-up view in Fig. 2.

In the inner section, a cohesive zone damage model is implemented by positioning zero-thickness cohesive elements that share the top nodes of the skin and the bottom nodes of the stringer. The element size of these cohesive elements is determined to be approximately 0.3 mm such that at least three cohesive elements are present in the cohesive processing zone [25]. The initiation in the elements is depicted by the quadratic stress criterion. The damage evolution follows the Benzeggagh-Kenane law [26] in order to capture the mixed mode behavior [27].

Table 1. Material properties of IM7/977-3.

Intralaminar properties				Interlaminar properties			
Longitudinal modulus	E_{11}	164000	MPa	**Mode I critical SERR**	G_{IC}	0.256	kJ/m^2
Transverse modulus	E_{22}	8980	MPa	**Mode II critical SERR**	G_{IIC}	0.65	kJ/m^2
Shear modulus	G_{12}	5010	MPa	**Mode I interface strength**	τ_{Ic}	78.9	MPa
Poisson's ratio	ν_{12}	0.32		**Mode II interface strength**	τ_{IIc}	99.4	MPa
Ply thickness	**t**	0.128	mm	**Benzeggagh-Kenane parameter**	η	2.07	

At both edges of the panel, where the stringers terminate, a clamped boundary conditions is applied while the edges parallel to the stringers are kept unconstrained. The panel is loaded in end-shortening by applying a displacement boundary condition at the far end of the panel along the stringers axis. A quasi-static displacement rate of 1 mm/s is chosen such that the kinetic energy is negligible with respect to the total strain energy.

The resulting force-displacement response of the four-stringer panel can be seen in Fig. 3a. Buckling is observed after an end-shortening of 0.7 mm. Small load drops around 3.3 mm applied displacement depict a loss of stiffness due to skin-stringer separation. This shows that the load carrying capability can extend far into postbuckling.

The buckling shape of the panel is shown in Fig. 3b and it consists of five half-waves. The four red areas within the inner section depict full separation while the blue areas are still intact. The common denominator for these locations is that they all originated at the inflection point of a buckling wave. At this point, the twisting of the skin results in high shear stresses at the interface creating a combined mode II + III opening. The evolvement of the separated areas can be divided into a sequence of four occurrences. This sequential occurrence can be attributed to the fact that separation is favored in the wider central skin bay and due to the position of the ±45º.

The separated areas in the model do not grow past the inside radius of the stringer, since the innermost element of the stringer is tied to the skin, arresting any growth. As a result, the extension of separation from one flange to the other cannot be captured. This phenomenon, also known as tunneling, could potentially lead to the collapse of the whole panel [4, 28]. However, the current approach does enable a single model to capture the eight locations of separation. Especially since these locations are all within 2% of the applied displacement of each other, any form of imperfections, e.g. geometrical or a damage, can result in another location being more critical in the stiffened panel. Based on these findings, a single-stringer specimen is designed in order to study the skin-stringer behavior under twisting deformation more closely.

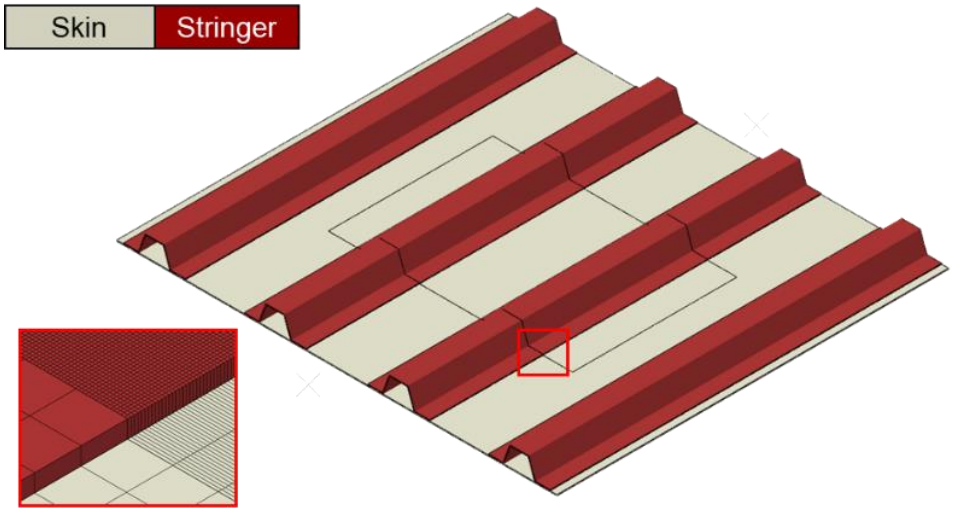

Fig. 2 Four-stringer panel.

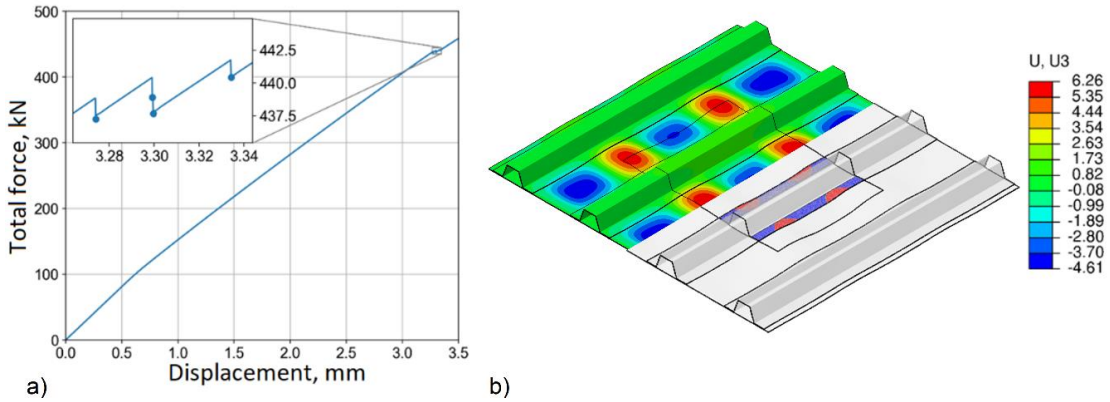

Fig. 3 Numerical results of four-stringer panel: a) force-displacement response, and b) out-of-plane buckling deformation and interface separation.

IV. Skin-Stringer Separation in a Single-Stringer Specimen

This section provides the FE prediction of skin-stringer separation in a single-stringer panel loaded in a four-point twisting deformation. The composite single-stringer specimen is designed to replicate the deformation and stringer separation characteristics of the four-stringer panel.

The length of this specimen is 140 mm, which is determined by the buckling half-wave length at the location of interest. The width of the specimen is 254 mm, which is approximately equal to the distance between the mid-points of two skin bays. The basic layout of this configuration is taken from the ECT coupon test [17-20], in which two supports and two loading points forces a coupon specimen in twisting. By changing the position of the loading points and supports in this layout, which are defined by the variables S_X and S_Y as shown in Fig. 4a, the difference between the out-of-plane deformation of the single-stringer specimen and the buckling shape of the four-stringer panel can be minimized [22]. The position variables are discretized in steps of 4 mm, and for each position, the shape difference is calculated. The shape difference is defined by the Residual Sum of Squares (RSS), also known as sum of squares of deviation, which is zero if there is a perfect fit [29]:

$$\mathrm{RSS} = \sum_{i=1}^{n} (y_i - x_i)^2 \tag{1}$$

In this equation, y_i and x_i are the nodal out-of-plane displacement for the four-stringer panel and the single-stringer approximation, respectively. A linear interpolator is applied to the results of the single-stringer specimen in order to match the relative spatial position of the nodes in the four-stringer panel model. A surface plot of the shape difference as a function of the two position variables is shown in Fig. 4b. For this four-point configuration the minimum difference is obtained at S_X = 44 mm and S_Y = 60 mm.

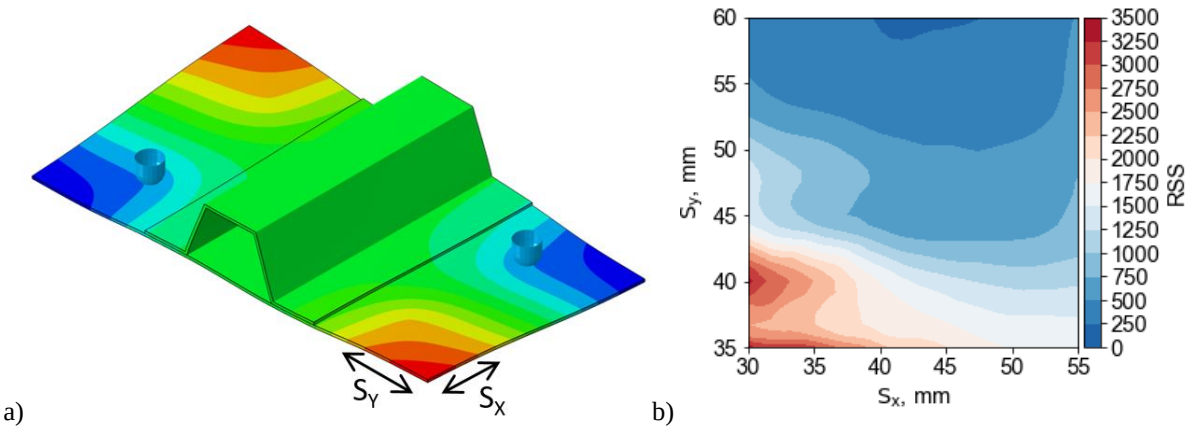

Fig. 4 Determining the loading point position: a) single-stringer specimen, and b) calculating the difference in out-of-plane deformation between the four-stringer panel and the single-stringer specimen for each layout.

The numerical model of the single-stringer specimen that is used to model skin-stringer separation includes COH3D8 elements for the interface and SC8R elements for the skin and stringer. The corners of the stringers are modelled with a radius of 5 mm. In this case the rounded corners are deemed necessary such that interface separation could initiate and/or propagate freely. The webs and top of the stringer and the skin thereunder exhibit no complex deformation or damage. A mesh transition zone is present just after the rounded corner, where in each row of this transition, the elements size is increased by a factor of three up to a mesh size of approximately 2 mm. The model of the specimen and a close-up of the interface, stringer radius and mesh transition are shown in Fig. 5.

The specimen is loaded via a contact constraint between the skin and hemispherical analytical rigid surfaces (ARSR) representing the loading points of the actual experimental set-up. The specified contact constraint is surface to surface with finite sliding in order to capture the change in contact state during the high skin deformation. Since the contact occurs between the flat skin and the curved surface of the loading points, a small element size is required for the contact region of the skin. The contact region is meshed with square elements of 0.3 mm, in accordance with the element size of the cohesive zone. The loading points move orthogonally to the skin surface, imposing the buckling-like deformation conditions at a rate of 4 mm/s onto the specimen.

Upon loading, the force-displacement response of the panel, which is presented in Fig. 6, displays an initial increase in stiffness. This phenomenon has also been observed in the research regarding the ECT test [17-20]. The initial small load drop at a displacement of 5.1 mm is attributed to the opening of the interface near the loading point, shown in Fig. 7a. At a displacement of 5.3 mm, shown in Fig. 7b, the crack progresses to the region of highest shear strain. At a displacement of 6.7 mm, shown in Fig. 7c, the interface near the rounded inside corner at the edge of the specimen starts to separate as well, due to a component of transverse shear. At a displacement of 7.4 mm, the crack fronts meet and the stringer almost completely separates from the skin.

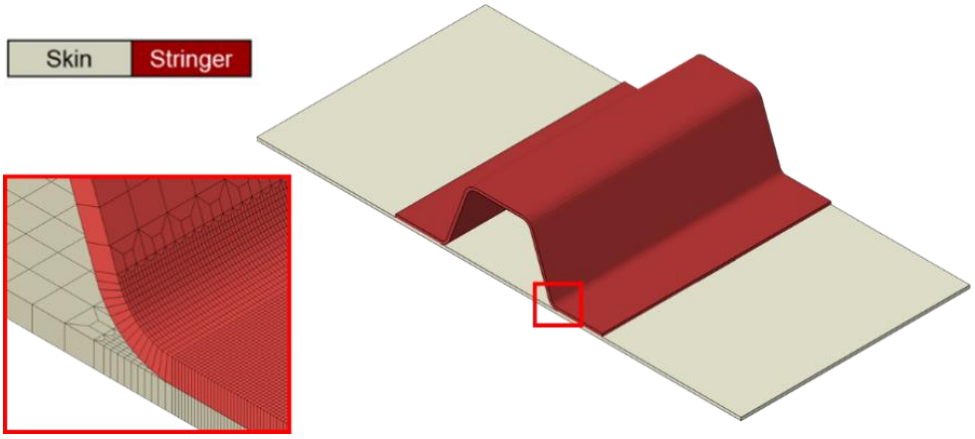

Fig. 5 Numerical model of the single-stringer specimen with cohesive zone model.

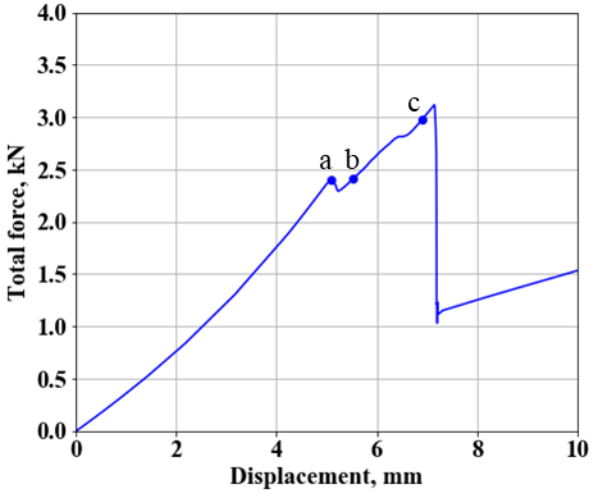

Fig. 6 Out-of-plane loading response of single-stringer specimen.

The mode mixity at the damage initiation (MMIXDMI) and damage evolution (MMIXDME) in the cohesive elements are presented in Fig. 8a and Fig. 8b, respectively. At a mode mixity value equal to negative one, the cohesive element is still intact. The SERR can be attributed fully to mode I at a mixed mode value equal to zero and to mode II/III at a value equal to one. The cohesive zone model does not distinguish in terms of input and output between mode II and mode III. However, it can be observed that damage initiation is mainly driven by these shearing modes. The eventual skin-stringer separation initiates as a result of peeling introduced by the loading points. Upon continued loading, the crack progresses, dominated by mode II + III, due to the twisting behavior of the specimen. The separation in the inner radius of the hat-stringer also initiates in mode II + III.

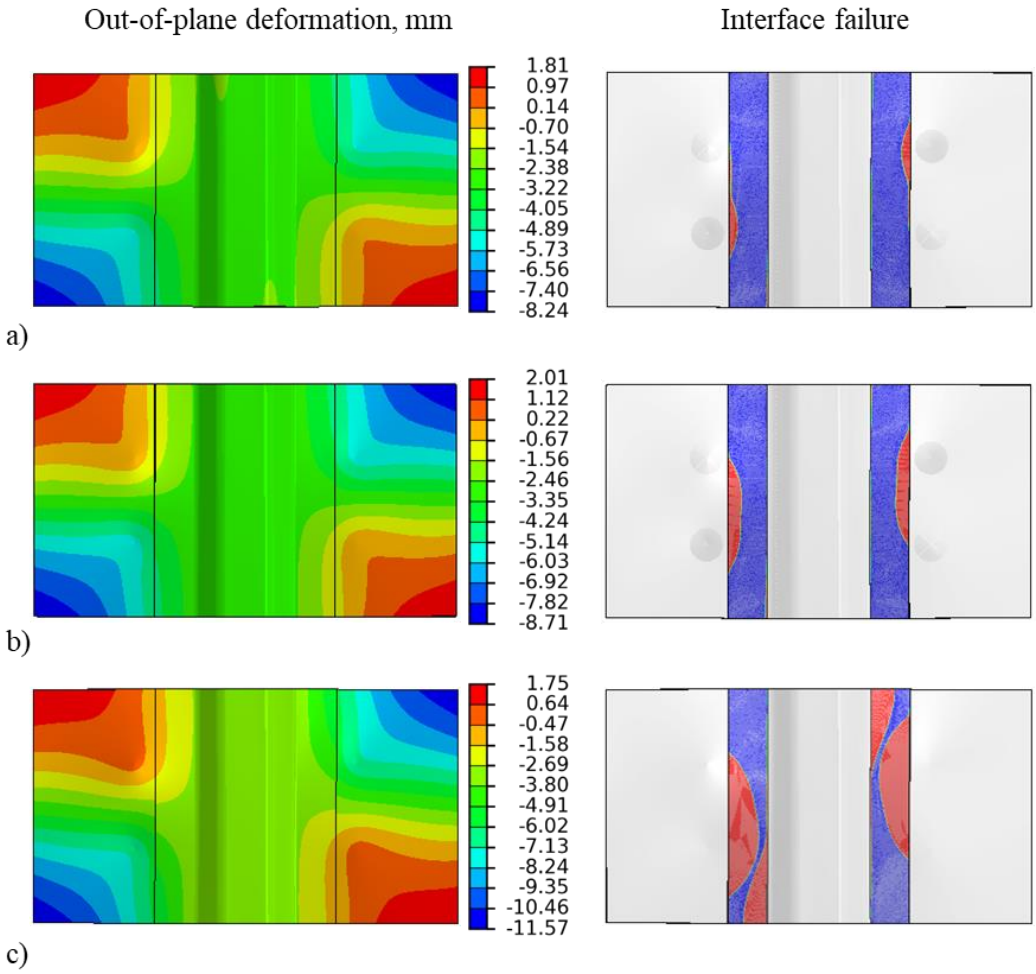

Fig. 7 Out-of-plane deformation and interface failure of single-stringer specimen at an applied displacement: a) 5.1 mm, b) 5.3 mm, and c) 6.7 mm.

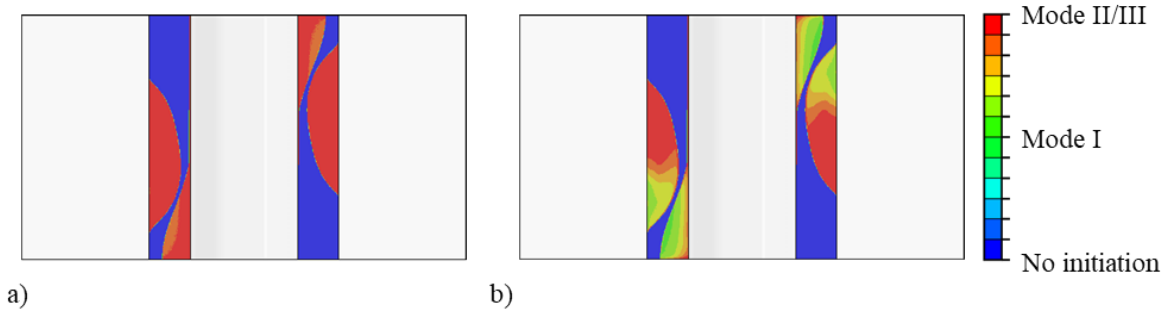

Fig. 8 Mode mixity of cohesive elements: a) damage initiation, and b) damage evolution.

V. Experimental Validation of Single-Stringer Specimen

A new adaptive multi-point test equipment has been designed to have the possibility to move the supports and loading points. This enables an adaptive configuration that can impose the most critical buckling deformation onto the single-stringer specimen. Using DIC and a C-scan device the displacement and strain results, as well as skin-stringer separation, can be compared to the numerical model.

A. Test Specimens and Equipment

The composite specimens are manufactured in-house at the Delft Aerospace Structures and Materials Laboratory. In total, four specimens are manufactured and two of them can be seen in Fig. 9. The first two specimens were used to study and validate the optimal configuration with S_X = 44 mm and S_Y = 60 mm. The distance between the stringer flange and the loading points is increased for the other two specimens, obtaining the configuration with S_X = 44 mm and S_Y = 50 mm. In addition, the free edges of the stringer flanges of the latter two specimens are clamped to prohibit the initiation of any mode I opening. An overview of the specimen layout can be found in Table 2.

The test equipment, including the two individual DIC systems, can be seen in Fig. 10a. DIC is used to track the out-of-plane deformation and the global strains of the single-stringer specimen. A close-up of the testing equipment can be seen in Fig. 10b, with the individual loading points and supports. Each support and loading point has its own load cell in order to track the loading distribution during the tests, which are numbered in Fig. 10c.

The bottom of the machine, on which the base plate is placed, moves upwards at a quasi-static displacement rate of 2 mm/min. The DIC system uses Vic-Snap as the acquisition software at a frequency of 0.5 Hz. After testing, the Vic3D 8 software is used to process the data and to calculate the strain, and VicPy is used for additional post-processing. The results of the two DIC systems are combined to get the full strain field of the skin-stringer overlap.

After audible cracking and visible load drops, the specimens are unloaded and removed from the fixture to obtain the ultrasonic C-scan. The C-scans are made with a Rollerform probe of 5 MHz and 64 elements. Then, the specimens are placed back and the load is increased. The load-displacement response, the delaminated areas and the DIC measurements are compared to the FE predictions.

Fig. 9 Single-stringer specimens.

Table 2. Overview of test specimens.

	S_X mm	S_Y mm	Length mm	Width mm	Skin thickness mm	Clamp
4PB1_60	44	60	140	254	1.58	None
4PB2_60	44	60	140	254	1.62	None
4PB1_50	44	50	140	254	1.53	Edge
4PB2_50	44	50	140	254	1.50	Edge

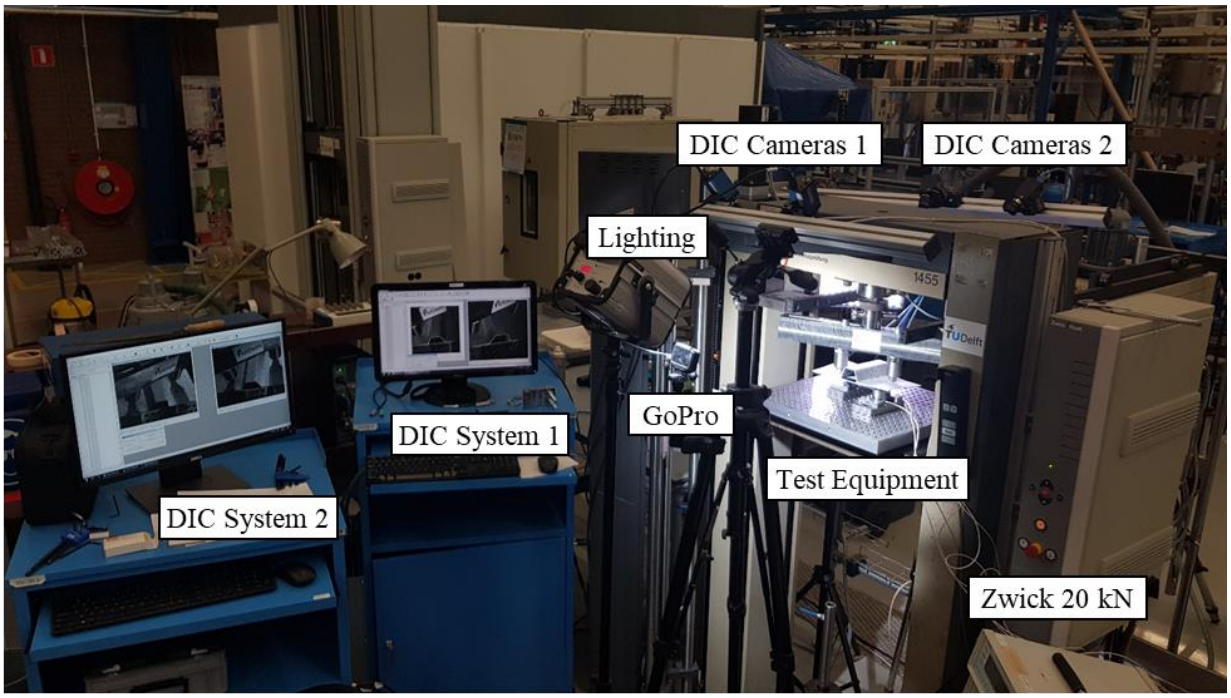

a)

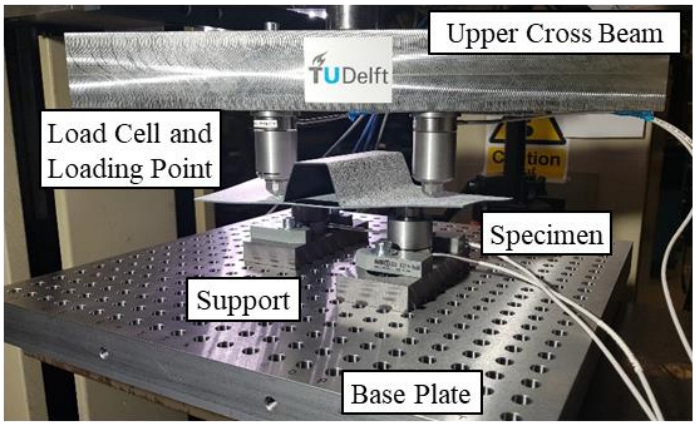

b)

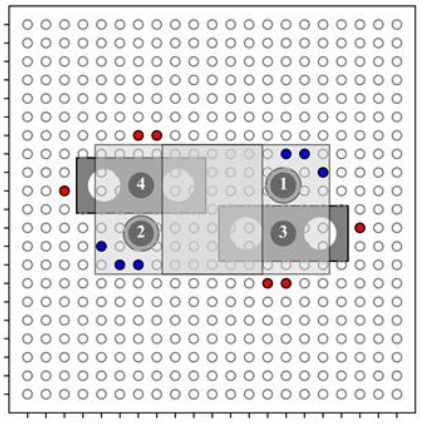

c)

Fig. 10 Adaptive multi-point test equipment: a) complete test set-up, b) close-up of equipment, and c) illustration of loading and support points.

B. Test Results of the Single-Stringer Specimen in the Optimal Configuration with S_Y = 60 mm

The load-displacement responses of 4PB1_60 and 4PB2_60 (defined in Table 2) are presented in Fig. 11a. It is observed that the removal of the specimen between the runs and reloading them has a minimal effect on the stiffness response for all the specimens. The first occurrence of audible cracking and a load drop due to this indentation is observed at an applied load of approximately 2 kN total force. After Run 1, all specimens displayed some small indentation damage due to applied pressure of the loading points, which is indicated by the dark blue sections in the C-scans presented in Fig. 12. The skin-stringer interface can be clearly distinguished by the red zones of approximately 3 mm depth. The light green parts depict a depth of 1.5 mm, which is the reflection of the skin portion only.

After the second run, specimens displayed that the stringer is separated from the skin at one side, where the red section in the pristine scans in Fig. 12 changed to green. This appears to be a combination of loading point induced peel stress and a shear induced separation, which is also observed in the numerical models. The loading distribution per loading point and support is shown in Fig. 11b, in which the load cell number corresponds to the numbering in Fig. 10c. The small difference in distribution of the loading may be attributed to the fact that the specimen was slightly curved in the out-of-plane direction. This difference might have led to the onset of separation at only one side of the specimen. After the third run, anti-symmetric separation is observed, which matches well with the FE prediction from Fig. 7c.

In order to compare the stiffness and final collapse to the FE model, a fourth loading run is performed for the 4PB2_60 specimen. The initial stiffness response of the experimental test and the FE analysis are visually similar, but started to deviate above 2 kN due to the indentation delamination adding compliance to the system. Both the skin-stringer separation and the collapse in the experiment occurred at a load that is about 50% higher than the FE prediction. Therefore, another analysis with cohesive elements with a mode II critical SERR of 1.95 kJ/m^2 was conducted. The FE results of the nominal and updated model are shown in Fig. 13 together with the response of the 4PB2_60 for run 1 and run 4.

The results agree with the published literature which states that the critical SERR used in FE model may be lower, specifically for mode II and mode III. These values can be different in the experimental case for numerous reasons: having a non standard +45/-45 interface combined with resistance curve effects that increase the critical SERR upon crack propagation [10] or not knowing the actual critical SERR for mode III [17-20]. All these uncertainties indicate that further research is still needed for structural panels that experience high twisting deformation due to buckling.

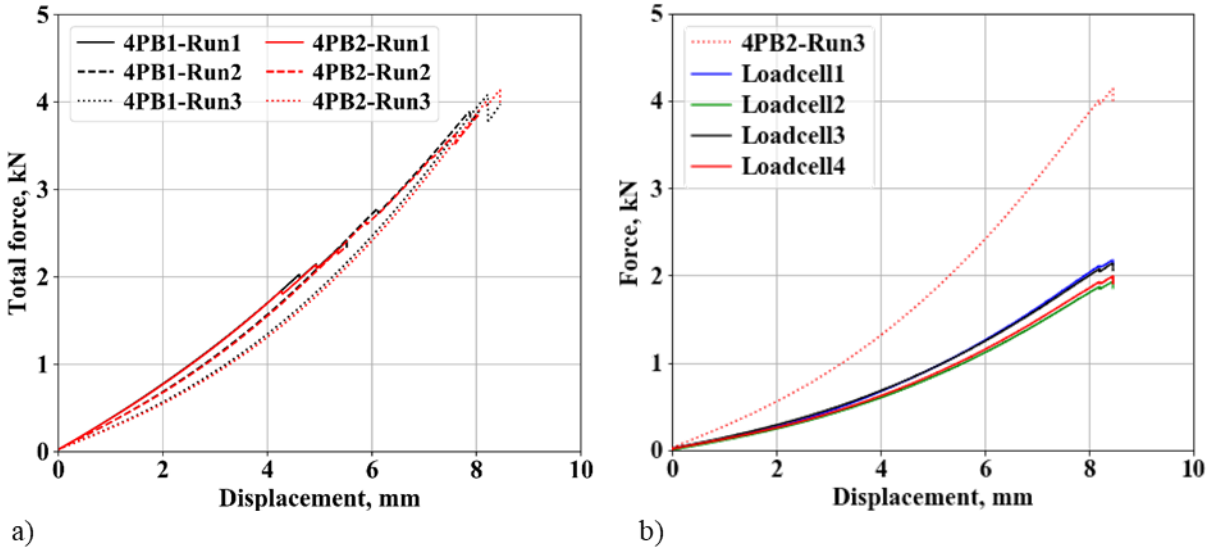

Fig. 11 Force-displacement response of single-stringer specimen: a) total force of 4PB1 and 4PB2, and b) total force and single loadcell force of 4PB2-Run3.

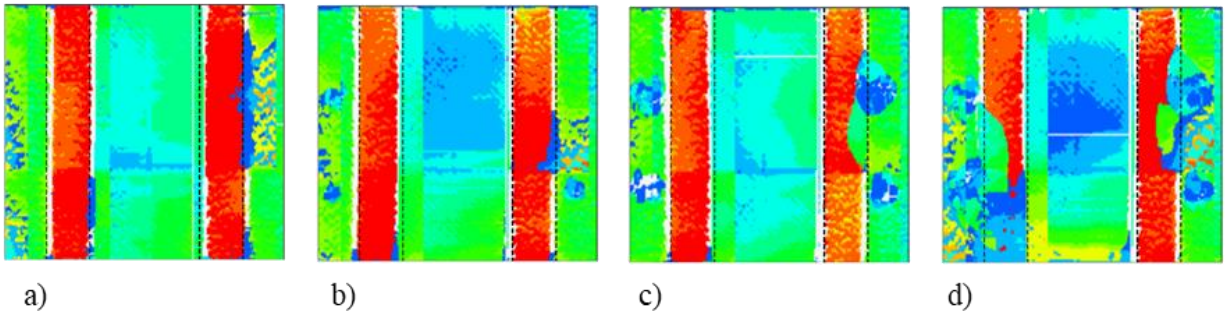

Fig. 12 C-scans of 4PB2: a) pristine panel, b) after run 1, c) after run 2, and c) after run 3.

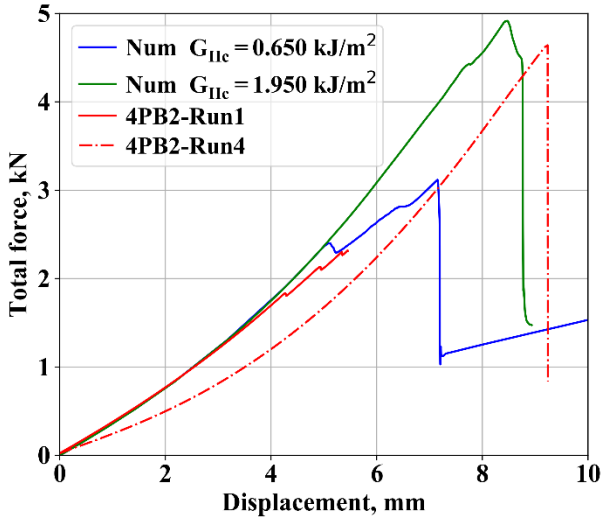

Fig. 13 Comparison between numerical and experimental force-displacement response.

C. Test Results of the Single-Stringer Specimens with S_Y = 50 mm and including Edge Clamps

The second set of tests is conducted with another two specimens, namely 4PB1_50 and 4PB2_50, aimed at predicting the skin-stringer separation without peel effect of the loading points on the stringer flange. The first deviation with respect to the initial design is the increase in distance between the loading points and the stringer flange. The second is the introduction of clamping at all four free edges of the stringer flange, each over a length of 10 mm.

The comparison between the FE prediction and the experimental results indicate a good stiffness match. Furthermore, there is a less pronounced increase in compliance due to loading point delamination, demonstrating the need for the larger distance between the loading points and the stringer flange. The FE models are only analyzed with the nominal critical SERR. The clamps are simulated in the FE model by replacing the cohesive elements at the edge by rigid body ties to prohibit both the mode I opening as well as opening due to shearing at the edges, which is illustrated in Fig. 14b. Nonetheless, the FE model over predicts failure with respect to the test results as shown in Fig. 14a, where the dots denote the maximum applied force. In the experiments, it is observed that separation can still occur due to a mode II component at the inner radius of the stringer, which is shown in Fig. 14c, despite the clamps at these locations. This has also been observed in the FE prediction of the optimal configuration, which is shown in Fig. 7.

At the points in Fig. 14a, the out-of-plane deformation and the longitudinal, transverse, and shear strain in the global reference frame are taken. These are shown in Fig. 15a for the FE model and in Fig. 15b for the DIC measurements of the 4PB2_50 specimen. The missing data in the results of the DIC measurement systems could arise from mainly the following obstructions: clamps at the edges, loading points, upper cross beam and the stringer webs that are parallel to the camera view. The out-of-plane deformation between FE and DIC is qualitatively similar, except for the additional out-of-plane components at the loading points. In case of the strain fields, the longitudinal and transverse strain of the FE model show similar behavior with respect to the test. However, the strain gradient at the loading points is higher in the FE model as there is a single point of contact. In case of shear strain, the experimental tests from Fig. 15d seems to experience a higher shear deformation compared to the FE model.

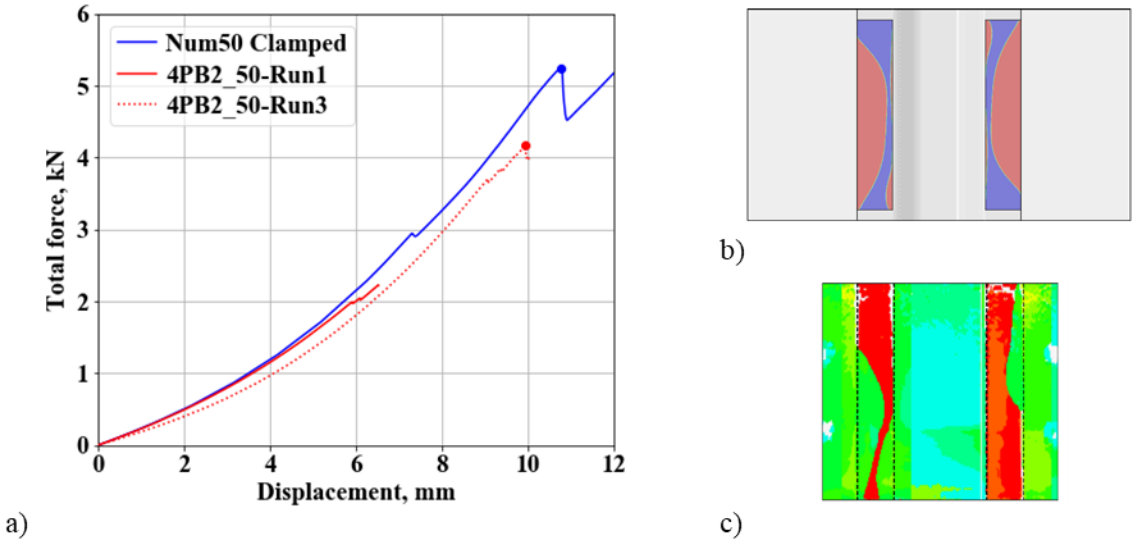

Fig. 14 Numerical-experimental comparison: a) force-displacement response, b) FE model interface separation, and c) interface separation of 4PB2_50.

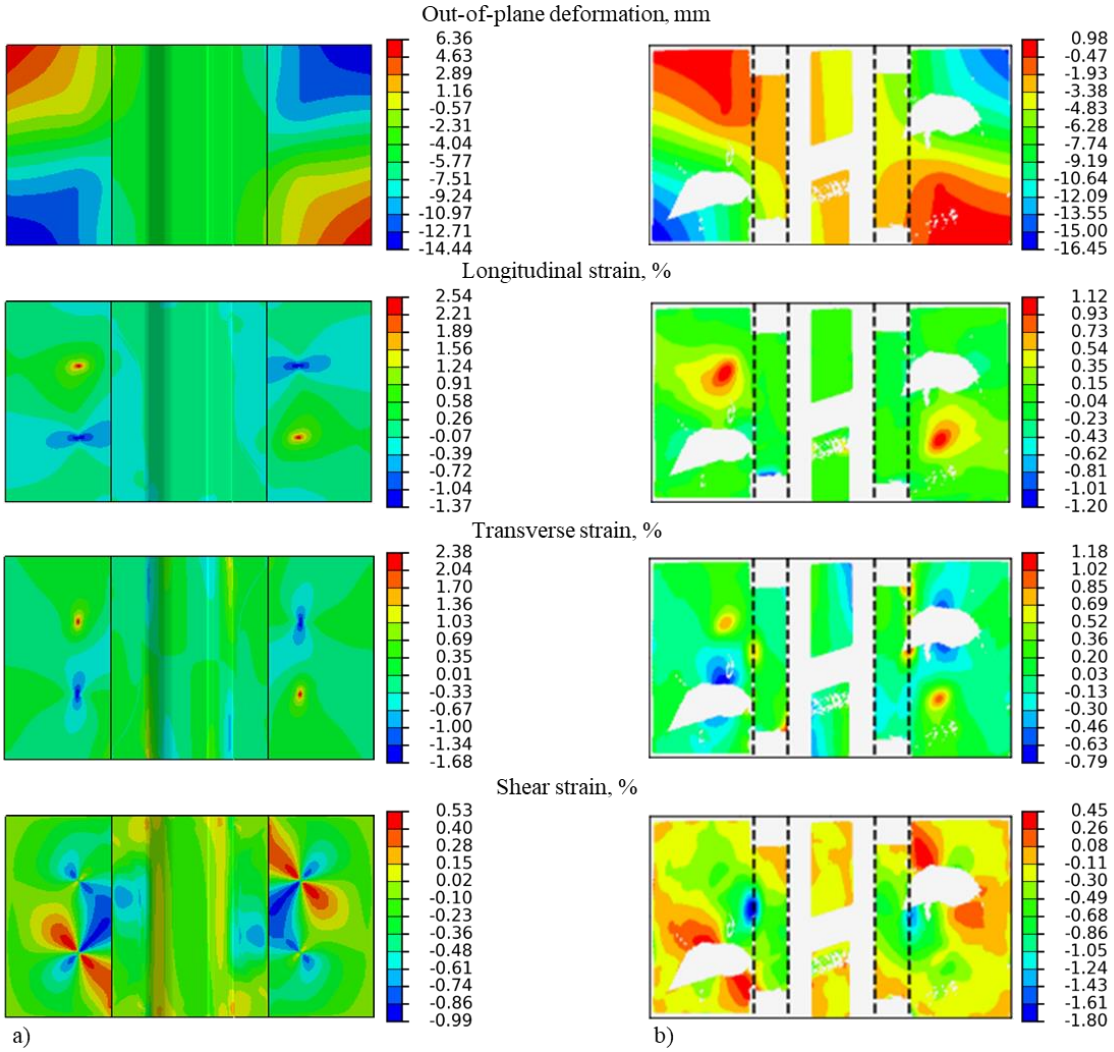

Fig. 15 Out-of-plane deformation and strains: a) numerical results and b) DIC measurements of 4PB2_50.

VI. Concluding Remarks

A new test methodology has been investigated to bridge the gap between coupon level testing and multi-stringer panel testing in the building block approach. The focus of this research is to capture the skin-stringer separation caused by high out-of-plane postbuckling deformations, which may lead to the collapse of the structure. Large aircraft panels are expensive and time consuming to model, manufacture, and test. The paper presented a novel four-point twisting configuration, inspired by the edge crack torsion coupon test, that is capable of capturing the combined mode II + III opening of the skin-stringer interface.

The finite element models of a single-stringer specimen in a four-point twisting configuration predicted that the failure occurs due to a combined mode II + III opening of the interface. However, the other failure modes such as crack initiation within the stringer interface at the edge of the specimen, may have taken place as well. Furthermore, it is deemed important to have sufficient distance between the stringer flange and the loading points in order to limit any mode I type opening of the interface that may interact with the desired mode II + III opening.

The experimental validation of these single-stringer specimens show good agreement with the finite element predictions in terms of initial stiffness and separation characteristics. Clamps at the free edges of the stringer flange limited the mode I opening, but may not prevent any shear type separation at the free edges. Furthermore, the finite element models under predicted the load at which separation occurs, which can be attributed to the reduced value of the critical strain energy release rate for the nonstandard interface that is loaded in combinations of mode II and III.

The paper shows that a configuration can be found that allows the approximation of the out-of-plane deformation of a postbuckled multi-stringer panel using a representative single-stringer specimen in an adaptive multi-point test equipment. The same test equipment can also be used to reproduce the most critical buckling deformation separation due to high out-of-plane bending in a seven-point bending layout using a single-stringer specimen. Future work is planned in order to extend the methodology and validate with different panel configurations. This will contribute to a better understanding and prediction of skin-stringer separation in large multi-stringer panels.

Acknowledgments

The authors gratefully acknowledge the financial support received from the European Office of Aerospace Research and Development (EOARD), United States Air Force, under the guidance of David Garner. Cleared for public release 88ABW-2019-4973.

Authors commend the technical guidelines received from Vipul Ranatunga and Stephen Clay of the Air Force Research Laboratory, Carlos Dávila and Cheryl Rose of NASA Langley Research Center, and Steven Wanthal of Boeing Research and Technology, and their continuous suggestions and supportive involvement in the project through the monthly meetings.

The authors like to thank Edgars Labans and Steven Doesburg of Delft University of Technology for the support in the design of the test equipment.

References

[1] Minguet P.J., and O'Brien T.K., "Analysis of Test Methods for Characterizing Skin/Stringer Debonding Failures in Reinforced Composite Panels," *Composite Materials: Testing and Design*: Twelfth Volume, ASTM International, 1996.

[2] Bisagni C., "Progressive Delamination Analysis of Stiffened Composite Panels in Post-Buckling," in *Proceedings of the AIAA/ASME/ASCE/AHS/ASC 47th Structures, Structural Dynamics and Materials Conference*, AIAA paper 2006-2178, 2006.

[3] Bisagni C., Vescovini R., and Dávila C.G., "Single-Stringer Compression Specimen for the Assessment of Damage Tolerance of Postbuckled Structures," *Journal of Aircraft*, 48(2):495-502, 2011.

[4] Bisagni C., and Dávila C.G., "Experimental Investigation of the Postbuckling Response and Collapse of a Single-Stringer Specimen," *Composite Structures*, 108:493-503, 2014.

[5] Dávila C.G., and Bisagni C., "Fatigue Life and Damage Tolerance of Postbuckled Composite Stiffened Structures with Indentation Damage," *Journal of Composite Materials*, 52(7):931-943, 2018.

[6] Van Rijn J.C.F.N., and Wiggenraad J.F.M., "A Seven-Point Bending Test to Determine the Strength of the Skin-Stiffener Interface in Composite Aircraft Panels," *NLR Technical Report* 2000-044, 2000.

[7] Bertolini J., Castanié B., Barrau J.J., and Navarro J.P., "Multi-Level Experimental and Numerical Analysis of Composite Stiffener Debonding. Part 1: Non-Specific Specimen Level," *Composite Structures*, 90(4):381-391, 2009.

[8] Bertolini J., Castanié B., Barrau J.J., Navarro J.P., and Petiot, C., "Multi-Level Experimental and Numerical Analysis of Composite Stiffener Debonding. Part 2: Element and Panel Level," *Composite Structures*, 90(4):392-403, 2009.

[9] Wanthal, S., Schaefer, J., Justusson, B., Hyder, I., Engelstad, S. and Rose, C.A., "Verification and Validation Process for Progressive Damage and Failure Analysis Methods in the NASA Advanced Composites Consortium," in *American Society for Composites (ASC) 32nd Technical Conference*, West Lafayette, 2017.

[10] Dávila C.G., Leone F.A., Song K., Ratclife J.G., and Rose C.A., "Material Characterization for the Analysis of Skin/Stiffener Separation," *Proceedings 32nd American Society for Composites Conference*, West Lafayette, IN., 2017.

[11] Zalameda, J., and Winfree, W., "Detection and Characterization of Damage in Quasi-Static Loaded Composite Structures Using Passive Thermography," *Sensors*, 18(10):3562-3579, 2018.
[12] Kosztowny, C.J.R., Dávila, C.G., Song, K., Rose, C.A., and Jackson, W., "Experimental and Numerical Analysis of Skin-Stiffener Separation Using a Seven-Point Bend Configuration," in *Proceedings of AIAA SciTech 2019*, 1767-1781, 2019.
[13] Falzon, B.G., Stevens, K.A., and Davies, G.O., "Postbuckling Behaviour of a Blade-Stiffened Composite Panel Loaded in Uniaxial Compression," *Composites Part A: applied science and manufacturing*, 31(5):459-468, 2000.
[14] Meeks, C. Greenhalgh, E., and Falzon, B.G., "Stiffener Debonding Mechanisms in Post-Buckled CFRP Aerospace Panels," *Composites Part A: applied science and manufacturing*, 36(7):934-946, 2004.
[15] Orifici, A.C., Ortiz de Zarate Alberdi, I., Thomson, R.S., and Bayandor, J., "Compression and Post-Buckling Damage Growth and Collapse Analysis of Flat Composite Stiffened Panels," *Composite Science and Technology*, 68(15-16):3150-3160, 2008.
[16] Vescovini, R., Dávila, C.G., and Bisagni, C., "Failure Analysis of Composite Multi-Stringer Panels using Simplified Models," *Composites: Part B*, 45(1):939-951, 2013.
[17] Lee, S.M., "An Edge Crack Torsion Method for Mode III Delamination Fracture Testing," *Journal of Composites Technology and Research*, 15(3):193-201, 1993.
[18] Li J., Lee S.M., Lee E.W., and O'Brien T.K., "Evaluation of the Edge Crack Torsion (ECT) Test for Mode III Interlaminar Fracture Toughness of Laminated Composites," *Journal of Composites, Technology and Research*, 19(3):174-183, 1997.
[19] de Morais, A.B., Pereira, A.B., de Moura, M.F.S.F., and Magalhães, A.G., "Mode III Interlaminar Fracture of Carbon/Epoxy Laminates Using the Edge Crack Torsion (ECT) Test," *Composites Science and Technology*, 69(5):670-676, 2009.
[20] Ratcliffe, J.G., "Characterization of the Edge Crack Torsion (ECT) Test for Mode III Fracture Toughness Measurement of Laminated Composites," *NASA/Technical Memorandum 213269*, 2014.
[21] Military. *CHM-17-3F: Composite Materials Handbook, Polymer Matrix Composites: Materials Usage, Design, and Analysis.* US Department of Defense, 2002
[22] Kootte, L.J., Bisagni, C., Dávila, C.G., and Ranatunga, V., "Study of Skin-Stringer Separation in Postbuckled Composite Aeronautical Structures," in *Proceedings of the American Society for Composites Thirty-third Technical Conference*, 1750-1761, 2018.
[23] Clay, S.B., and Knoth, P.M., "Experimental Results of Quasi-Static Testing for Calibration and Validation of Composite Progressive Damage Analysis Methods," *Journal of Composite Materials*, 51(10):1333-1353, 2017.
[24] ABAQUS/Standard User's Manual, Version 2019. Simulia, 2019.
[25] Turon, A., Dávila, C.G., Camanho, P.P., and Costa, J., "An Engineering Solution for Mesh Size Effects in the Simulation of Delamination Using Cohesive Zone Models," *Engineering Fracture Mechanics*, 74(10):1665-1682, 2007.
[26] Benzeggagh, M.L., and Kenane, M., "Measurement of Mixed-Mode Delamination Fracture Toughness of Unidirectional Glass/Epoxy Composites with Mixed-Mode Bending Apparatus," *Composite Science and Technology*, 56(4):439–449, 1996.
[27] Turon, A., Camanho, P.P., Costa, J., and Renart, J., "Accurate Simulation of Delamination Growth under Mixed-Mode Loading Using Cohesive Elements: Definition of Interlaminar Strengths and Elastic Stiffness," *Composite Structures*, 92(8):1857-1864, 2010.
[28] Van Dooren, K.S., Labans, E., Tijs, B.H.A.H., Waleson, J.E.A., and Bisagni, C., "Analysis and Testing of a Thermoplastic Composite Stiffened Panel under Compression," In *ICCM22-22nd International Conference on Composite Materials, Melbourne*, Australia, 2019.
[29] Draper, N.R., and Smith, H., *Applied Regression Analysis*, 3rd ed., John Wiley and Sons, Chap. 1, 1998